SAND2024-05052C

Sandia National Laboratories

TIME-VARIABLE MOMENT TENSOR INVERSION OF SEISMIC AND SEISMOACOUSTIC DATA AT THE SOURCE PHYSICS EXPERIMENT PHASE II: DRY ALLUVIUM GEOLOGY

Andréa Darrh[1], Elizabeth Berg[1], Leiph A. Preston[1], Christian Poppeliers[1,2,3]
[1]Sandia National Laboratories, Albuquerque, New Mexico, [2]Leidos, Patrick Space Force Base, Florida, [3]Air Force Technical Applications Center, Patrick Space Force Base, Florida

Introduction

In many applications, seismic sources can be represented as a moment tensor acting at a point in the Earth. Each component of the moment tensor represents a force couple with, in general, an independent source time function (STF). Traditionally, however, the same analytic STF is assumed for all components and full waveform inversions only solve for the scalar moment. These inversions can therefore underestimate the complexity of a source if secondary events in time occur, for example, explosion-induced slip on near-source joints after an explosion.
The time-variable moment tensor (TVMT) inversion (e.g., Poppeliers *et al.*, 2018; Berg and Poppeliers, 2022) solves for an independent STF for each moment tensor component that best fits the observed data. The TVMT inversion honors greater source complexity by 1) allowing the estimated source mechanism to evolve through time, 2) removing the constraint that the STF is identical for each component of the moment tensor, and 3) not requiring a source time function template to find a solution. In this work, we conduct our TVMT inversions using data from the Source Physics Experiment Phase II: Dry Alluvium Geology (DAG) to characterize the evolution of the DAG-4 source with time.

Inversion formulation

Seismic data ($\boldsymbol{u}$) can be represented as a convolution of Green's functions describing the response of the Earth between a source location ($\boldsymbol{x}$) and the location of the k^{th} receiver ($\boldsymbol{x}'$), with the n^{th} force couple (m) (Aki and Richards, 2002)

$$u_k(\boldsymbol{x}', \boldsymbol{t}) = \sum_{n=1}^{6} \int_{-\infty}^{\infty} g_{k,n}(\boldsymbol{x}', \boldsymbol{t}; \boldsymbol{x}, \boldsymbol{t}) m_n(\boldsymbol{x}, \boldsymbol{t}) dt,$$

which can also be expressed in matrix form as $\boldsymbol{u} = \boldsymbol{Gm}$, where $\boldsymbol{m}$ is the STF associated with the six unique moment tensor components.
The deterministic individual inversions are constructed as a regularized modified least-squares, minimizing an objective function ϕ

$$\min \phi = \left\| \boldsymbol{w}(\boldsymbol{Gm} - \boldsymbol{u}^{obs}) \right\|_2^2 + \lambda \|\boldsymbol{W}_m \boldsymbol{m}\|_2^2,$$

where $\boldsymbol{w}$ is a weighting function applied to the observed and predicted seismic data, $\boldsymbol{G}$ is the Green's function matrix, $\boldsymbol{u}^{obs}$ is the observed data, λ is the Lagrange parameter, and $\boldsymbol{W}_m$ is the model weighting matrix, $\boldsymbol{W}_m^T \boldsymbol{W}_m = \alpha^2 \boldsymbol{I} + \beta^2 \boldsymbol{L}^T \boldsymbol{L}$, comprised of two weighting terms α and β and a second-derivative Laplacian matrix $\boldsymbol{L}$. The seismic data and Green's functions are windowed using a weighting function, $\boldsymbol{w}$ (Harding *et al*., 2023), which applies a unity weight function until 0.5 s after the P-wave first arrival for a given waveform, after which a unit-amplitude half-Gaussian is applied with a 0.8 s standard deviation. The weighting function, $\boldsymbol{w}$, is unity for infrasound data. The solution for a range of λ values are evaluated with the final result selected using the L-curve criterion. Prior to inversion, the observed data from the DAG-4 explosion is filtered using a sixth order Chebyshev bandpass from 0.5 to 4 Hz and resampled to a 50 samples/s sample rate.
We conduct three inversions: 1) an individual inversion inverting just seismic data, 2) an individual inversion inverting infrasound data, and 3) a novel joint inversion formulation where the STF solution from the individual seismic inversion is used as a priori information in an infrasound inversion. We refer to this latter formulation as a "sequential seismoacoustic inversion" stated as

$$min\, \phi = \left\| \boldsymbol{G}_A \boldsymbol{m}_A - \boldsymbol{u}_A^{obs} \right\|_2^2 + \lambda \left\| \boldsymbol{W}_m (\boldsymbol{m}_A - \boldsymbol{m}_{ref}) \right\|_2^2.$$

The reference model, $\boldsymbol{m}_{ref}$, is set equal to the seismic STF solution. The final model is selected using the minimum of the combined data misfits $\phi_d^{comb} = \left\| \boldsymbol{G}_A \boldsymbol{m}_A - \boldsymbol{u}_A^{obs} \right\|_2^2 + \gamma \left\| \boldsymbol{G}_S \boldsymbol{m}_S - \boldsymbol{u}_S^{obs} \right\|_2^2$ where infrasound is denoted with subscript A and seismic with subscript S. The weight on the seismic data objective function is approximately equal to the ratio between the infrasound data misfit and the seismic data misfit. The station locations used in all TVMT inversions are shown in Figure 1.

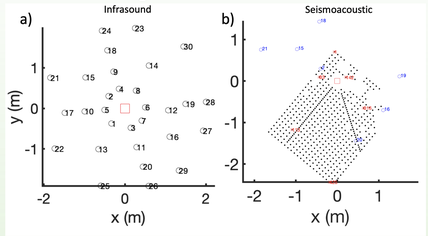

Figure 1: Location of infrasound and seismic stations used in the TVMT inversions.

Green's functions

The seismic and infrasound Green's functions were created using Parelasti, a 3D finite difference solution to the elastic wave equation (Poppeliers and Preston, 2021). The same 3D geologic model (Figure 2) was used to generate the seismic and infrasound Green's functions used in all inversion cases and was created using the geologic framework model for the region (Protho & Wagoner, 2020). The air speed used for the model was 347 m/s and was calculated using the temperature and the specific humidity recorded for DAG-4.

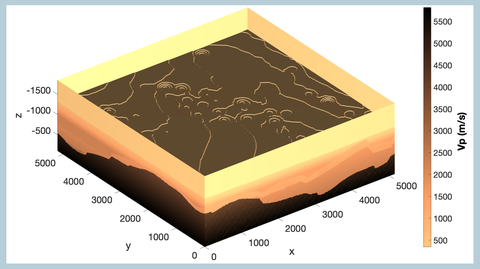

Figure 2: 3D model displaying the P-wave velocities used to generate the seismic and infrasound Green's functions used in the three inversions. Layer depths and velocities are based on the geologic framework model of the area (Prothro & Wagoner, 2020). The model is cut at the surface to show the topography of the area.

TVMT inversion results

Seismic-only, infrasound-only, and seismoacoustic inversion results obtained using combinations of seismic and acoustic data collected from DAG-4 (Figures 3-5). The TVMT inversion results are output as moment rate functions, integrated, and shown here as moment functions. The moment function results are plotted on fundamental lunes (Tape and Tape, 2012) to characterize the time evolution of the DAG-4 source.

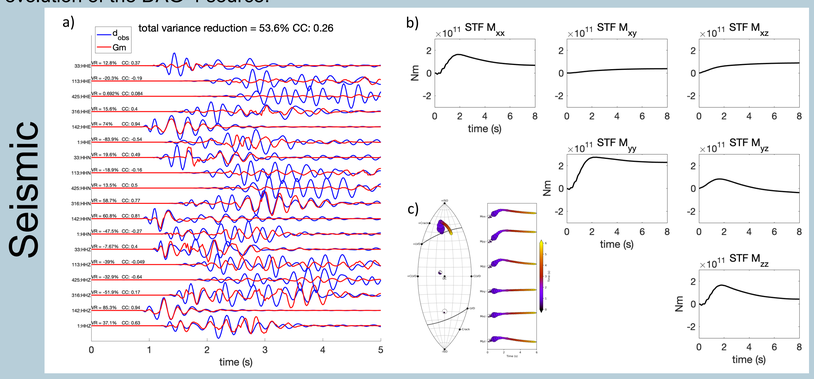

Figure 3: Seismic-only TVMT inversion result. a) Predicted (red) and observed data (blue), the variance reduction (VR), and correlation coefficient (CC) for each station and the overall fit stated at the top. b) Moment function results for the six unique moment tensor components. c) Moment function result plotted on a fundamental lune.

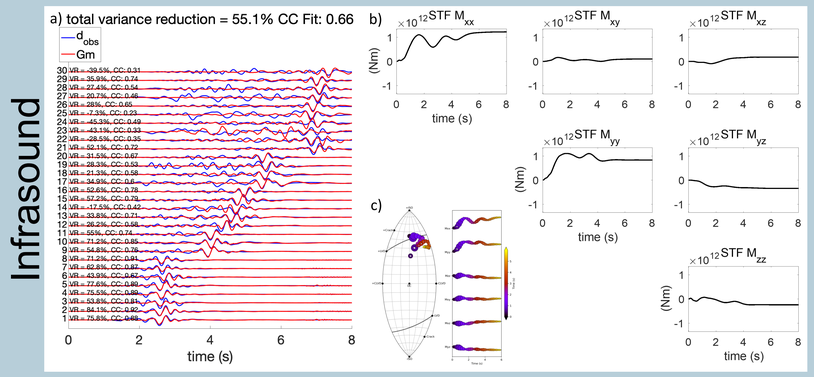

Figure 4: Infrasound-only TVMT inversion result. a) Predicted (red) and observed data (blue), the variance reduction (VR), and correlation coefficient (CC) for each station and the overall fit stated at the top. b) Moment function results for the six unique moment tensor components. c) Moment function result plotted on a fundamental lune.

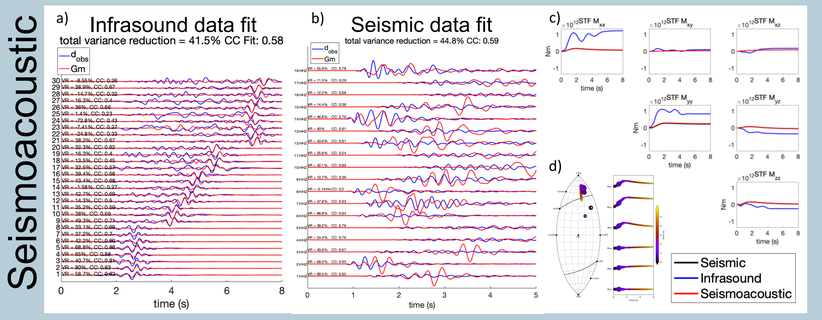

Figure 5: Seismoacoustic TVMT inversion result. a) Predicted (red) and observed data (blue), the variance reduction (VR), and correlation coefficient (CC) for each station and the overall fit stated at the top. b) Predicted seismic data (red) using the seismic Green's functions (GFs) and seismoacoustic STF result, plotted with the observed seismic data (blue). All data fit measures are evaluated for a 0.5 second window centered around the first arrival. c) Moment function results for the six unique moment tensor components for the seismic-only (black), infrasound-only (blue), and seismoacoustic inversion (red). d) Seismoacoustic moment function result plotted on a fundamental lune.

Discussion

The seismic-only, infrasound-only, and seismoacoustic inversions all produced moment functions that appear isotropic, with the seismic moment function initially plotting along the negative half of the fundamental lune, but plotting positively isotropic after ~0.5 s. This is likely due to an oscillation present in the beginning of the seismic moment function result, an artifact of the windowing used for the seismic data. The infrasound-only inversion has a second peak in the moment function results at ~ 3.5 seconds that is not observed in the seismic-only results. The seismoacoustic inversion, while resulting in a slightly lower variance reduction for the infrasound-only inversion, has a comparable correlation coefficient fit. The results obtained from the seismoacoustic inversion are similar to those obtained from the seismic-only inversion while still allowing for the epicentral acoustic arrival to be fit by the predicted data.
The main findings of this work are summarized as follows:

- The amplitude of the moment function estimated by the infrasound-only inversion is an order of magnitude larger than the seismic-only moment function and has two prominent peaks
- A sequential inversion where the infrasound data were inverted using the seismic STF as a reference model resulted in a final moment function that was very similar to that recovered from the seismic-only inversion and which reasonably fits the epicentral acoustic arrivals.
- The seismoacoustic STF results in predicted data that reasonably fit the first arrivals of the seismic data, especially for the closer stations. This suggests that the seismoacoustic inversion result retains the early-time characteristics of the seismic moment function while still reasonably fitting the infrasound data.

Acknowledgements

This Source Physics Experiment (SPE) research was funded by the National Nuclear Security Administration, Defense Nuclear Nonproliferation Research and Development (NNSA DNN R&D). The authors acknowledge important interdisciplinary collaboration with scientists and engineers from LANL, LLNL, NNSS, and SNL.

References:
Aki, K. and Richards, P. G. (2002). *Quantitative seismology*. University Science Books, 2 edition.
Berg, E. and Poppeliers, C. (2022). Unraveling the Wrinkle in Time-Variable Sources with Lunes and Synthetic Seismic Data. Technical Report SAND2022-13242, Sandia National Lab. (SNL-NM), Albuquerque, NM (United States).
Harding, J. L., Preston, L. A., and Eliassi, M. (2023) The influence of physical and algorithmic factors on simulated far-field waveforms and source–time functions of underground explosions using unsupervised machine learning, *Geophysical Journal International*, Volume **233**, Issue 2, Pages 1399–1415, https://doi.org/10.1093/gji/ggac510
Poppeliers, C., Aur, K. A., and Preston, L. (2019). The Relative Importance of Assumed Infrasound Source Terms and Effects of Atmospheric Models on the Linear Inversion of Infrasound Time Series at the Source Physics Experiment. *Bulletin of the Seismological Society of America*, **109**(1):463–475. doi: https://doi.org/10.1785/0120180249
Poppeliers, C., and L. Preston (2021). The effects of earth model uncertainty on the inversion of seismic data for seismic source functions, *Geophys. J. Int.*, **224**(1), 100-120, https://doi.org/10.1093/gji/ggaa408.
Prothro, L. B., & J. Wagoner (2020). Geologic framework model for the Dry Alluvium Geology (DAG) experiment testbed, Yucca Flat, Nevada National Security Site. United States. https://doi.org/10.2172/1670996
Tape, W. and Tape, C. (2012). A geometric setting for moment tensors. *Geophysical Journal International*, **190**(1):476–498.

U.S. DEPARTMENT OF ENERGY
National Nuclear Security Administration
Sandia National Laboratories is a multimission laboratory managed and operated by National Technology & Engineering Solutions of Sandia, LLC, a wholly owned subsidiary of Honeywell International Inc., for the U.S. Department of Energy's National Nuclear Security Administration under contract DE-NA0003525.
SAND2024-05052C
Sandia National Laboratories